CONF-820609--82

OPTIMIZATION OF A BUNDLE DIVERTOR FOR FED*

L. M. Hively, General Electric Company/Fusion Engineering Design Center
K. E. Rothe, Oak Ridge National Laboratory
M. Minkoff, Argonne National Laboratory

CONF-820609--82

DE83 017255

*Research sponsored by the Office of Fusion Energy, U. S. Department of Energy, under contract No. W-7405-eng-26 with the Union Carbide Corporation.

ABSTRACT

Optimal double-T bundle divertor configurations have been obtained for the Fusion Engineering Device (FED). On-axis ripple is minimized, while satisfying a series of engineering constraints. The ensuing non-linear optimization problem is solved via a sequence of quadratic programming subproblems, using the VMCON algorithm. The resulting divertor designs are substantially improved over previous configurations.

I. INTRODUCTION

Bundle divertors are being studied as one means of active control for impurities, as well as for shielding the first wall from particle and heat fluxes. External magnet coils create a field that opposes the tokamak toroidal field. Divertor control is then a result of plasma particles following the field lines past the separatrix and into a collector/pumping zone (1). In comparison to poloidal divertors (2), bundle divertors are more compact and do not link other magnetic coils, allowing size reductions in the toroidal field (TF) and poloidal field (PF) coils. Although there is a large, local perturbation due to the TF null of a bundle divertor, access is easier for vacuum pumping and maintenance. Also, a bundle divertor appears capable of protecting the first wall throughout a burn cycle. However, the operation of a poloidal divertor is sensitive to variations in both the plasma and PF coil currents, making wall protection difficult.

Past bundle divertor studies have concentrated on engineering aspects of bundle divertor design (see, for example, Ref. 3), but more recent works have also included the physics effects of magnetic ripple (4-9). While only Refs. 4-6 assess the qualitative effects of ripple on plasma transport, all agree that adverse effects decrease with lower ripple. In their study of ergodicity and magnetic island formation in the plasma equilibrium as well as fast ion confinement, Yang et al. (7) demonstrate markedly reduced ripple effects by examining various bundle divertor configurations. Bateman and Theriault (8) have studied a variety of hybrid bundle divertor designs to obtain low ripple configurations. However, Refs. 7-8 do not consider ripple optimization of a fixed configuration. Our previous study (9) focussed on engineering-constrained ripple optimization of the double-T bundle divertor and obtaining very low ripple designs with minimal ripple effects. Moreover, we showed that divertor-created, on-axis ripple above 0.3% causes the loss of most banana-trapped fast ions. These losses would be unacceptable in the Fusion Engineering Device (FED) using quasi-perpendicular injection or ion cyclotron resonance heating. In addition, these designs (of Ref. 9) require large, expensive copper coils, which would dissipate >100 MW of resistive power. Consequently, a bundle divertor is now considered only as a backup option to a poloidal divertor in FED.

The present work extends the effort of Ref. 9, using an improved optimization technique. The ripple optimization model is summarized in Sect. II, and the resulting optimization problem is described in Sect. III. The results are presented in Sect. IV along with our conclusions.

II. RIPPLE OPTIMIZATION MODEL

Both fast ion and background plasma confinement may be degraded by divertor ripple. Nonaxisymmetry in a diverted tokamak causes fast ion losses due to particle trapping in localized magnetic wells. In one process, an ion can be collisionlessly trapped due to its finite orbit size when there is insufficient parallel velocity (at a banana tip) to escape from a ripple well. Such a ripple-trapped ion oscillates within the well, while drifting vertically into larger ripple, and is lost to the wall. Another process is collisional ripple trapping due to pitch-angle scattering at a banana tip. Collisional detrapping can occur by the inverse process. There is also banana-drift diffusion because large banana-width orbits fail to close exactly in the presence of ripple. This arises from a ripple-induced variable lingering period as the banana tip passes through a magnetic well. Usually, the bundle divertor produces a local maximum in B on each side of the ripple well, yielding a new ripple-induced trapping process. In particular, a particle can become banana-trapped between the divertor-created maximum and the usual 1/R increase in the toroidal field and then rapidly drifts out of the tokamak. These mechanisms cause outward radial transport and loss of fast ions, thus degrading plasma heating by neutral beams, fusion products, and rf heating.

Also, ripple degrades background plasma confinement by enhancing the coefficients for ion heat conduction and spatial diffusion. A badly designed divertor may ergodize the equilibrium field lines, causing further deterioration in plasma confinement or even inducing plasma disruptions. While these deleterious influences are not well

tested experimentally, it is prudent on theoretical grounds to assume that such effects are important. Consequently, minimizing divertor-induced ripple leads to a conservative set of optimization criteria.

The optimization model minimizes on-axis ripple by varying nine design parameters, subject to the following engineering constraints (see Fig. 1):

(1) a magnetic coil current density of 6 kA/cm^2,

(2) the front T-coil lying outside the scrape-off zone,

(3) the (a) vertical and (b) horizontal hole clearances through the divertor coils larger than chosen values,

(4) no interference between the front and back T-coils, and

(5) the innermost edge of the flux bundle lying beyond the back T-coil.

Although the algorithm of Ref. 9 imposed several equality restrictions, such equality constraints are unnecessary. However, in the course of minimizing ripple subject to these constraints via the present method, several of the constraints (2 and 3a in the front T-coil) are satisfied as equalitites within 10^{-3}-10^{-4}. The coil currents are chosen so that the separatrix joins the plasma edge far from the divertor. The total magnetic field is the sum of an axisymmetric, noncircular equilibrium field and the vacuum divertor field, which is calculated using the Biot-Savart law assuming filamentary coils. Toroidal field ripple is presently excluded, making the current results pessimistic. Details of the model are presented in Ref. 9 and will not be repeated here.

The ripple is calculated by integrating toward the divertor along a field line, beginning at a point far from the divertor. The resulting peak-to-average ripple δ is $(B_{max} - B_{min})/(B_{max} + B_{min})$, where B_{max} and B_{min} are the maximum and minimum values of the field strength along the field line. The positive ripple δ^+ is defined as $(B_{max} - B_o)/B_o$; similarly, negative ripple δ^- is given by $(B_o - B_{min})/B_o$. Here, B_o is the average field strength along the field line. For the best ion confinement, Bateman et al. (4) suggest that more weight be given to minimizing δ^- than δ^+. However, our work shows that minimizing either δ^+ or δ^-, while holding δ below a fixed value, yields essentially the same optimum as minimizing δ. In addition, confinement studies of such minimum-δ designs show excellent fast ion confinement (9). Therefore, we have chosen to minimize δ, subject to the above engineering constraints.

III. COMPUTATIONAL PROBLEM

A computer code DIVOPT has been developed to solve the double-T bundle divertor optimization problem. The code in its original form (9) required 60-90 cpu min on the CDC7600 at the Magnetic Fusion Energy Computer Center (MFECC) at Livermore, California. By changing the code from the CHATR compiler (10) to the FTN compiler (11), the computational speed was increased by a factor of 4-5. An additional two-fold speed improvement was obtained by calculating the vacuum divertor field from current loops using the BLOOPS routine (12) rather than from the simple sum of many straight wire filaments. Finally, the

NAGLIB optimizer E04UAF (13) was replaced by VMCON (14), which yielded a further speed increase of 4-5 fold, accompanied by substantially lower ripple divertor designs. The remainder of this section discusses some of the present optimization techniques and the considerations that led to the use of VMCON for the FED divertor optimization.

The general nonlinear programming problem (NLP) can be written as

$$\begin{aligned} &\text{Minimize } f(x) \\ &\text{subject to} \\ &\quad c_i(x) = 0 \qquad i = 1, \ldots, k \\ &\quad c_i(x) \geq 0 \qquad i = k+1, \ldots, m \ , \end{aligned} \tag{1}$$

where x is an n-vector of unknown variables, i.e., $x \in R^N$. Each of the functions $f: R^N \to R^1$ and $c_i: R^N \to R^1$ are assumed the be continuous and differentiable. Frequently, in order to assure convergence rate properties for an algorithm, it is necessary to assume continuous second or higher order derivatives.

There are many special cases of Eq. (1) that are useful in themselves and easier to solve, e.g., linear programming, quadratic programming, and linearly constrained nonlinear programming. We will have occasion to deal with convex quadratic programming (QP) subproblems later in this section. These problems have the form

$$\begin{aligned} &\text{Minimize } \frac{1}{2} x^T Q x + c^T x \\ &\text{subject to} \\ &\quad Ax \ \# \ b \ , \end{aligned} \tag{2}$$

where Q is an $n \times n$ positive definite matrix, c is an n-vector, A is an $n \times n$ matrix, b is an m vector and # is an m-vector of relations.

The components of # are "$\geq$", "$\leq$", or "=" and denote the nature of the m linear constraints in Eq. (2). One of the virtues of QP problems is that unlike a Newton's method algorithm (which involves an infinite sequence of iterations), algorithms to solve QP exist that require only a finite number of steps (15).

A solution x* to NLP must satisfy the first-order necessary conditions. Furthermore, algorithms to solve NLP attain convergence by satisfying the Kuhn-Tucker (KT) conditions (16), which are

$$\nabla f(x^*) - \sum_{i=1}^{m} \lambda_i^* \nabla c_i(x^*) = 0 \qquad (3a)$$

$$\lambda_i^* \geq 0 \qquad i = k+1, \ldots, m , \qquad (3b)$$

$$\lambda_i^* c_i(x^*) = 0 \qquad i = 1, \ldots, m , \qquad (3c)$$

$$c_i(x^*) = 0 \qquad i = 1, \ldots, k , \qquad (3d)$$

$$c_i(x^*) \geq 0 \qquad i = k+1, \ldots, m , \qquad (3e)$$

where λ^* is the vector of Lagrange multipliers. Notice that Eqs. (3d) and (3e) provide for feasibility of x*. Equation (3c) ensures the complementary nature of λ_i^* and $c_i(x^*)$. Equation (3a) can be interpreted as

$$\nabla_x L(x^*, \lambda^*) = 0 , \qquad (4)$$

where

$$L(x, \lambda) = f(x) - \sum_{i=1}^{m} \lambda_i c_i(x) \ . \qquad (5)$$

See Ref. 16 for further discussion of the KT conditions.

With the above background we can now consider algorithms to solve NLP. The field of algorithm and software development for solving NLP is an active and dynamic one. While we will mention only two approaches, there are many more (e.g., see surveys of Refs. 15 and 17). Techniques for solving NLP frequently deal with generating sequences of easier-to-solve subproblems. The first approach begins from the observation that in solving NLP we are simultaneously trying to do two things: minimize f(x) and satisfy the constraints. If we could formulate a single function to minimize, or even a sequence of such subproblems, then unconstrained minimization techniques could be applied. This approach is the basis of penalty functions (18) and augmented Lagrangian (15) methods. The augmented Lagrangian techniques are more recent and do not possess asymptotic ill-conditioning properties that penalty functions possess. In either case, a sequence of unconstrained problems are generated and can be solved (16) using standard techniques (usually conjugate-gradient, quasi-Newton, or Newton-like algorithms).

The second approach to solving NLP deals with solving sequences of QP subproblems. After each QP is solved a line search is conducted (i.e., a function of a single variable is minimized) to determine the new solution estimate. There are various specific algorithms based on this approach, some of which are discussed in the surveys of Refs. 15, 17, and 19. The specific algorithm that we will discuss is based on one given by Powell (15) and implemented in the software package VMCON (14).

The QP subproblem is obtained by approximating the Lagrangian in Eq. (5) with a positive definite quadratic function and linearizing the constraints about the solution estimate for the j^{th} iteration (x^j). The solution of QP provides estimates of the Lagrange multipliers λ^j and a search direction vector δ^j. The line search involves minimizing a function $\phi(x^j + \alpha\delta^j)$, which is chosen to balance the desire to minimize $f(x)$ and to satisfy the constraints. Note that α controls the step-length in the direction δ^j and is the independent variable in the line search. The specific form of the function is

$$\phi(x^j + \alpha\delta^j) = f(x) + \sum_{i=1}^{k} \mu_i^j |c_i(x)| + \sum_{i=k+1}^{m} \mu_i^j |\min[0, c_i(x)]| \quad , \quad (6)$$

where $x = x^j + \alpha\delta^j$ and μ^j is an m-component vector defined as

$$\mu_i^1 = |\lambda_i^1|$$

$$\mu_i^j = \max[|\lambda_i^j|, \tfrac{1}{2}(\mu_i^{j-1} + |\lambda_i^j|)], \quad j > 1 \; . \qquad (7)$$

μ^j is chosen to ensure that as j increases the constraints will be more nearly satisfied. The function in Eq. (6) is nondifferentiable, and this complication is dealt with in VMCON. After a new point is found with an α^j that improves Eq. (6) sufficiently, we use $x^{j+1} = x^j + \alpha^j\delta^j$ for the next QP. Notice that it is not necessary to minimize Eq. (6) but just to find an improved point.

To conclude the description of the VMCON algorithm we return to the QP subproblem. If the objective function in QP was truly a quadratic approximation of the Lagrangian, it would be necessary to

provide second-order information about f and c_i, i.e., $\nabla_{xx} f(x)$ and $\nabla_{xx} c_i(x)$ at each iteration. Instead, we use quasi-Newton methods to update the matrix Q. Thus, Q is a quasi-Newton estimate of $\nabla_{xx} L(x, \lambda)$, and we only need $f(x)$, $c_i(x)$ and their gradients to use VMCON. (For the FED optimization we use finite-difference estimates of these gradients.) At the conclusion of the line search we have x^{j+1} and x^j available in the form:

$$\xi = x^{j+1} - x^j, \quad \gamma = \nabla_x L(x^{j+1}, \lambda^j) - \nabla_x L(x^j, \lambda^j) . \tag{8}$$

A standard unconstrained quasi-Newton method (16) is then used to obtain an updated value of Q, Q_{NEW}, for the next QP subproblem:

$$Q_{NEW} = Q - \frac{Q\xi\xi^T Q}{\xi^T Q \xi} + \frac{\gamma\gamma^T}{\xi^T \xi} . \tag{9}$$

For use in VMCON the formula for γ is modified to ensure that Q remains positive definite (see Ref. 14). The initial estimate of Q is any positive definite symmetric matrix. While the identity is used as a default-starting matrix in VMCON, it is important to take the actual problem scaling into account in generating this initial estimate of $\nabla_{xx} L(x, \lambda)$.

Finally, we conclude this section with some comments about algorithm evaluation. The process of evaluting algorithms and software for solving NLP is quite complex and is, in itself, an important research subject. Clearly, no single software package will outperform all others on all problems. Thus, when examining evaluation data one

should be careful to examine the nature and structure of the test problems etc. (see Refs. 20 and 21). Nevertheless, in terms of function and gradient evaluations, which are the sources of most of the computational cost in the FED optimization, VMCON requires from 3-20 times fewer evaluations than a reduced gradient method (20). In comparing VMCON-like techniques with penalty/augmented Lagrangians, Schittkowski (21) obtains similar statistics. These results are consistent when we consider the nature of the algorithms involved. The penalty/augmented Lagrangian methods use function evaluations to obtain an accurate minimum to each unconstrained subproblem and then generate a completely new unconstrained problem to solve. VMCON-like methods do not use function evalutions while solving the QP subproblem. The reduced gradient methods, which are a third approach to solving NLP (16) and have been popular during the past decade, spend a large portion of their function evaluations in retaining feasibility as the algorithm proceeds. VMCON-like algorithms gradually attain feasibility and thus use their function evaluations more efficiently.

IV. RESULTS AND CONCLUSIONS

For FED (22), constrained optimization of an unshielded, double-T bundle divertor yields very low ripple designs, as shown in Fig. 2. Nuclear shielding is not required for the divertor because FED is a subignition device. Optimal designs were obtained for a high-beta (6%) FED equilibrium so the magnetic axis is shifted outward into the higher ripple region by 0.2 m. Compared to the results of Ref. 9, the ripple values in Fig. 2 are lower by a factor of 2-3 for the

0.3 × 0.4 m bore designs. However, 0.05-0.08 m of structure would be required around the coils (not included in the model of Ref. 9). The corresponding bore size would then be an unrealistically small value of 0.14 × 0.24 m. The optimal 0.5 × 0.6 m bore divertor was not obtainable using the optimization method of Ref. 9. This design (see Fig. 3) has a realistic bore of 0.34 × 0.44 m when structure is included, having a magnetic scrape-off thickness of 0.22 m. The corresponding power dissipation is 86 and 161 MW in the front and back T-coils, respectively. However, there is sufficient space to add nuclear shielding to the back T-coil for superconducting operation. This design would fit between two adjacent TF coils; additional coils would be needed to expand the diverted flux bundle near or beyond the outer legs of the TF coils. The resulting contours of constant ripple (see Fig. 4) are nearly vertical, with an exponential decrease from the outboard plasma edge (δ = 30%) to the magnetic axis (δ = 0.093%).

The confinement of collisionless, neutral-beam-injected, 150-keV D^+ ions has been calculated using a field line orbit code (23). For nonoptimal divertors with on-axis ripple above 0.3%, most of the bananas are lost; circulating ions are well-confined. For the optimal cases, only bananas with tips in higher ripple regions (δ > 0.4%) are lost; see Fig. 4 for results from the large bore case, described above. These loss orbits are usually D-shaped or small bananas, having tips outboard from the magnetic axis. Evaluation of collisional confinement for fast ions in a diverted plasma is in progress. Fast ions resulting from near-tangential injection are expected to be well confined.

In conclusion, significant improvements in low ripple bundle divertor configurations have been obtained, yielding much better designs than previous efforts. Such designs are compact and fit between adjacent TF coils. While experiments using high ripple divertors on DITE will clarify the deleterious ripple effects, the present lack of definitive results should not prejudice future work on advanced divertor designs.

REFERENCES

1. P. E. Stott, C. M. Wilson, and A. Gibson, Nucl. Fusion 17, 481 (1977).
2. D. Meade et al., in Proc. Plasma Phys. and Controlled Nuclear Fusion Research Vol. 1 (International Atomic Energy Agency, Vienna 1975), p. 605.
3. T. F. Yang et al., Westinghouse Electric Corporation, WFPS-TME-104, 1978.
4. G. Bateman, P. Theriault, and R. N. Morris, Proceedings of the Fourth Topical Meeting on Technology of Controlled Nuclear Fusion Vol. 2, Conf-801011, 1980, p. 1143.
5. G. Bateman and R. N. Morris, Georgia Institute of Technology, GTFR-15, 1980.
6. T. F. Yang et al., Massachusetts Intitute of Technology, PFC/JA-80-32, 1980.
7. T. F. Yang et al., Massachusetts Institute of Technology, PFC/JA-81-4, 1981.

8. G. Bateman and P. Theriault, Nucl. Tech./Fusion 2, 96 (1982).

9. L. M. Hively et al., Nucl. Tech./Fusion 2 (to be published).

10. L. Berdahl, Lawrence Livermore National Laboratory, UCID-18369, 1978.

11. LANL Fortran Extended Reference Manual, LA-5525-M. Vol. 3, June 1980.

12. D. K. Lee, Oak Ridge National Laboratory, ORNL/CSD/TM-104, 1981.

13. Numerical Algorithms Group (USA) Inc., 1250 Grace Court, Downers Grove, Illinois.

14. R. L. Crane, K. E. Hillstrom, and M. Minkoff, Argonne National Laboratory, ANL-80-64, 1980.

15. M. J. D. Powell, Mathematical Programming 14, 224 (1978).

16. M. Avriel, Nonlinear Programming Analysis and Methods (Prentice-Hall, New York, 1976).

17. M. Minkoff, "Nonlinear Constrained Optimization Methods," in Modeling and Simulation, Vol. 10, edited by W. G. Vogt and M. H. Mickle (Instrument Society of America, 1979), pp. 861-865.

18. A. V. Fiacco and G. P. McCormick, Nonlinear Programming: Sequential Unconstrained Minimization Techniques (John Wiley and Sons, New York, 1968).

19. P. E. Gill, W. Murray, M. A. Saunders, and M. H. Wright, "QP-based Methods for Large-scale Nonlinearly Constrained Optimization," in Nonlinear Programming 4, edited by O. L. Mangasarian, R. R. Meyer, and S. M. Robinson (Academic Press, New York, 1981), p. 57.

20. M. Minkoff, "Methods for Evaluating Nonlinear Programming Software," in Nonlinear Programming 4, edited by O. L. Mangasarian, R. R. Meyer, and S. M. Robinson (Academic Press, 1981), p. 519.

21. K. Schittkowski, Nonlinear Programming Codes, Lecture Notes in Economics and Mathematical Systems, Vol. 183 (Springer-Verlag, 1980).

22. C. A. Flanagan et al., Oak Ridge National Laboratory, ORNL/TM-7948, 1981.

23. R. H. Fowler et al., Oak Ridge National Laboratory, ORNL/TM-6293, 1978.

FIGURE CAPTIONS

Fig. 1. Schematic drawing of double-T bundle divertor, including the optimizable dimensions: R_1, L_1, D_1, R_2, L_2, and D_2; the coil heights H_1 and H_2 are not shown.

Fig. 2. On axis-ripple, δ, for an optimized double-T bundle divertor on FED versus scrape-off thickness T_{so} for 0.3 × 0.4 m and 0.5 × 0.6 m (width × height) free bores through the coils.

Fig. 3. Detailed configuration for the large-bore, double-T bundle divertor, showing field lines and coil parameters.

Fig. 4. Contours of constant ripple for the large-bore divertor of Fig. 3 with a high-β (β = 6%) FED equilibrium. Collisionless confinement of 150-keV D^+ ions has been calculated; each letter indicates the position of the banana tip for ion orbits that are ripple trapped (R) and lost, well-confined (C), and ergodic (E) for which confinement must be evaluated collisionally.

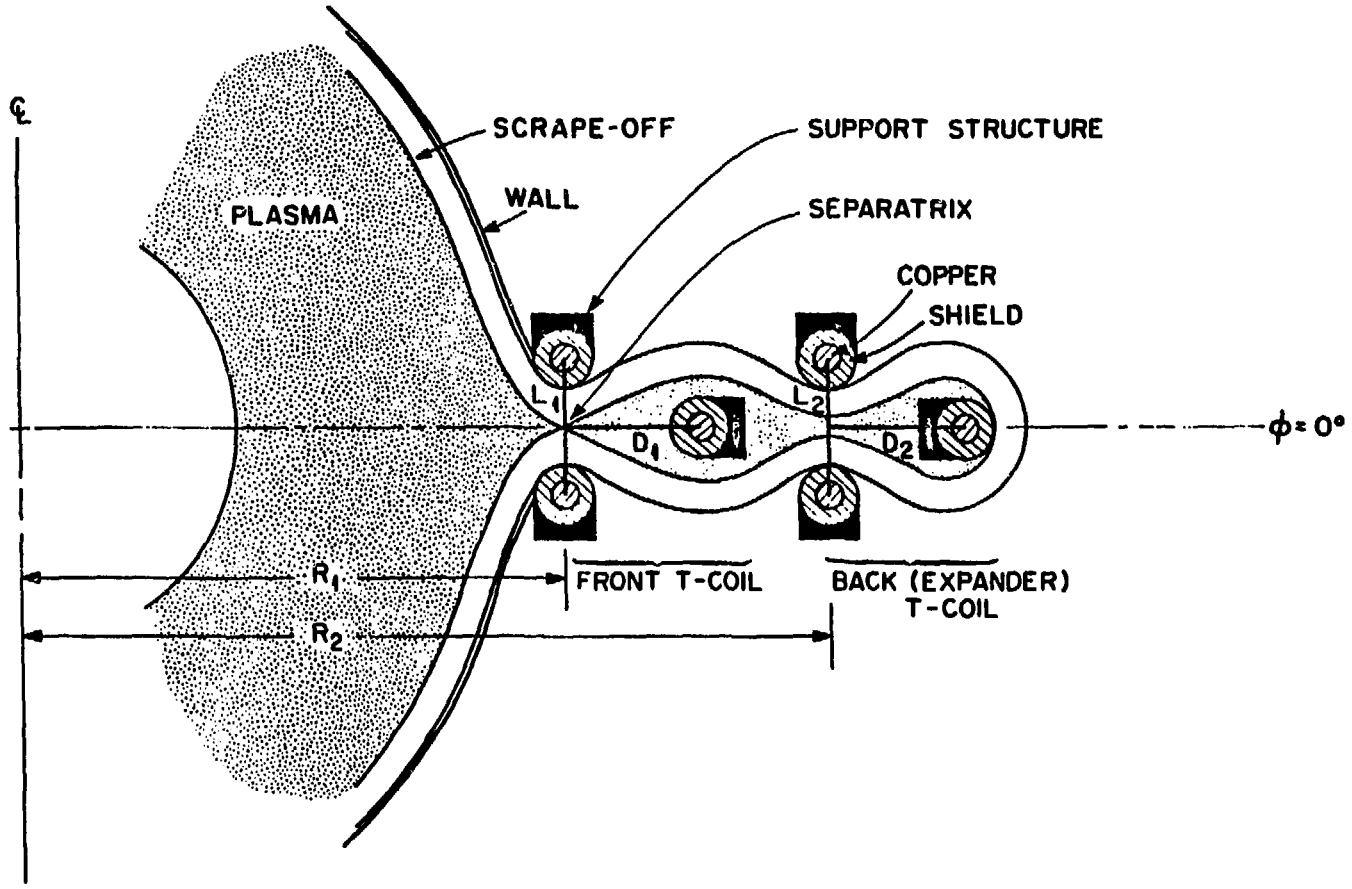
ORNL-DWG 80-3220R3 FED
SCRAPE-OFF
SUPPORT STRUCTURE
WALL
SEPARATRIX
PLASMA
COPPER
SHIELD
L1
L2
D1
D2
ϕ = 0°
R1
R2
FRONT T-COIL
BACK (EXPANDER)
T-COIL

Figure 1

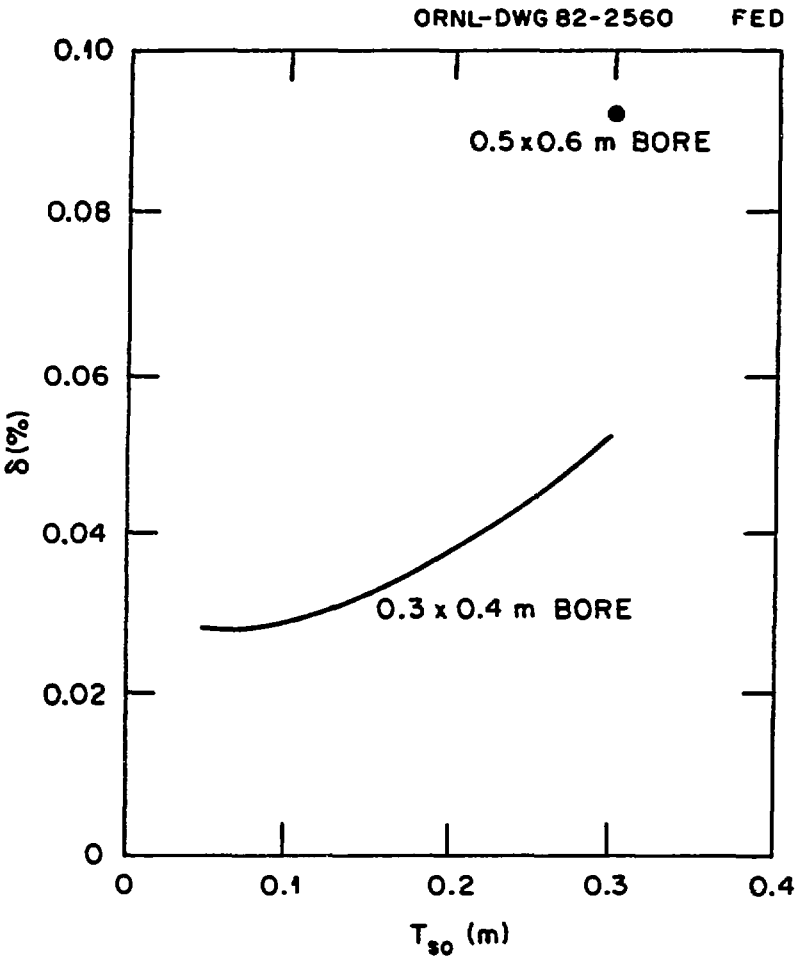
ORNL-DWG 82-2560 FED
0.10
0.08
0.06
0.04
0.02
0
δ(%)
0.5 x 0.6 m BORE
0.3 x 0.4 m BORE
0
0.1
0.2
0.3
0.4
T_{so} (m)

Figure 2

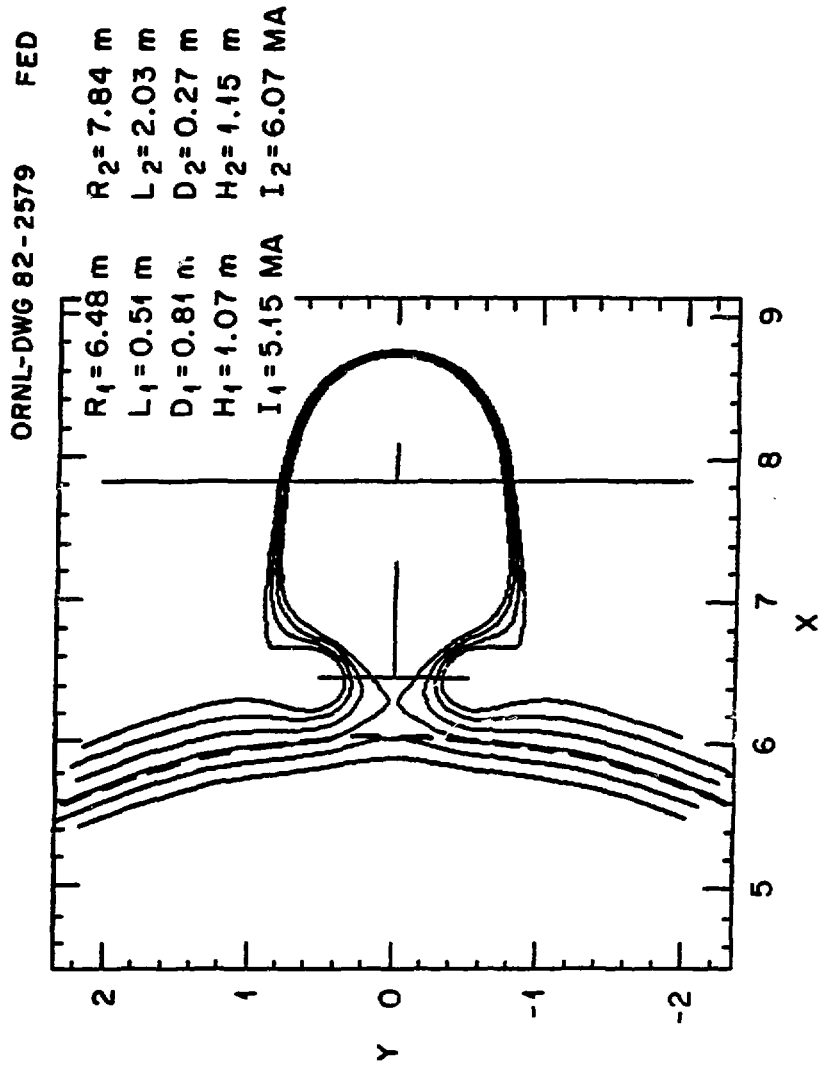
ORNL-DWG 82-2579 FED
R1=6.48 m R2=7.84 m
L1=0.51 m L2=2.03 m
D1=0.81 m D2=0.27 m
H1=1.07 m H2=1.15 m
I1=5.15 MA I2=6.07 MA
9
8
7
6
5
X
2
1
0
-1
-2
Y

Figure 3

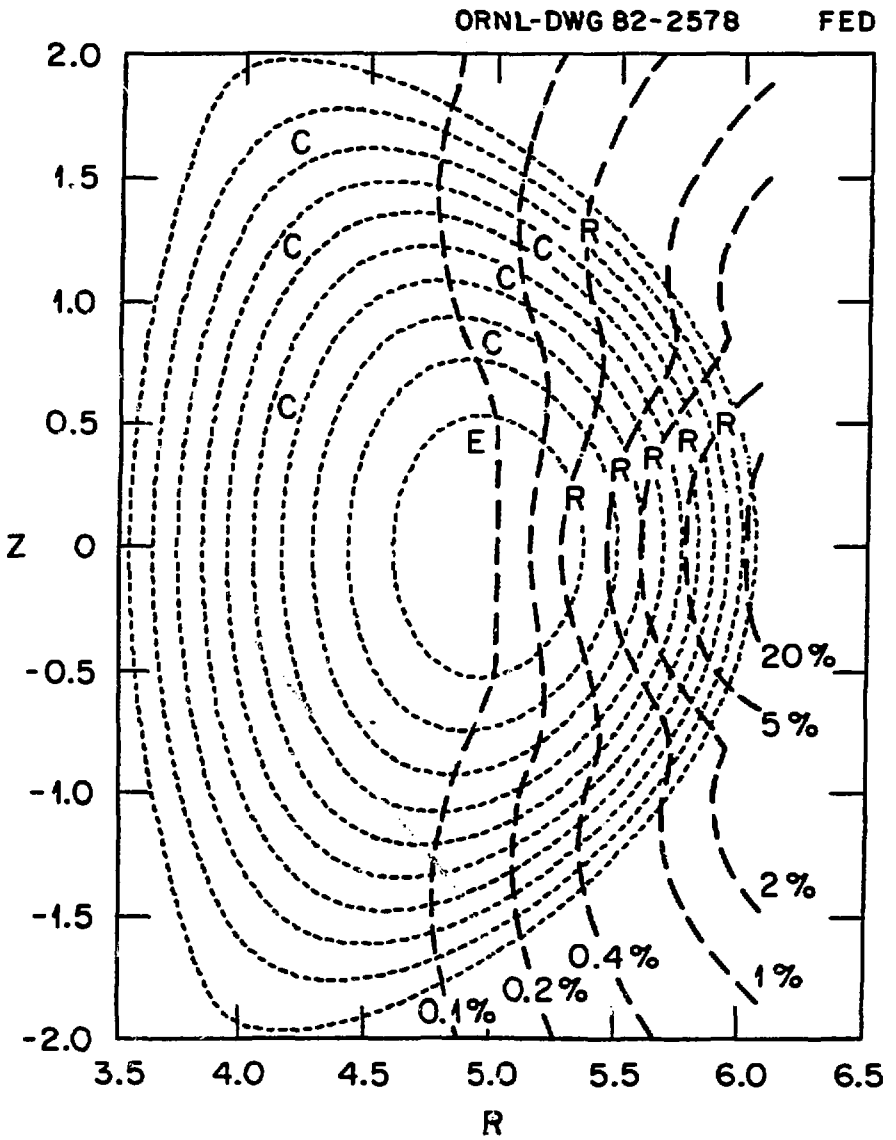
ORNL-DWG 82-2578
FED
2.0
1.5
1.0
0.5
Z 0
-0.5
-1.0
-1.5
-2.0
3.5
4.0
4.5
5.0
5.5
6.0
6.5
R
C
C
C
C
C
C
R
R
R
R
R
R
E
20%
5%
2%
1%
0.4%
0.2%
0.1%

Figure 4